MOLECULAR IMAGING AND BIOLOGY

Mol Imaging Biol (2017)
DOI: 10.1007/s11307-017-1158-7

RESEARCH ARTICLE

Fluorescence Molecular Imaging and Tomography of Matrix Metalloproteinase-Activatable Near-Infrared Fluorescence Probe and Image-Guided Orthotopic Glioma Resection

Li Li,[1,2] Yang Du,[2] Xinjian Chen,[1] Jie Tian[2]

[1]*School of Electronic and Information Engineering, Soochow University, No. 1 Ten Azusa Street, Suzhou, 215006, China*
[2]*CAS Key Laboratory of Molecular Imaging, The State Key Laboratory of Management and Control for Complex Systems, Institute of Automation, Chinese Academy of Sciences, No. 95 Zhongguancun East Road, Haidian District, Beijing, 100190, China*

Abstract

Purpose: Malignant gliomas are major causes of cancer-related mortality and morbidity. Traditional surgery usually leads to incomplete resection of gliomas resulting in the high incidence of tumor recurrence. Advanced medical imaging technology, such as fluorescence imaging-guided surgery, combined with tumor-specific imaging probes allows the identification of tumor margins and improved surgery. However, there are two pressing issues that need to be addressed: first, few fluorescence imaging probes can specifically target gliomas; second, fluorescence molecular imaging (FMI) cannot get the in-depth information of deep-seated gliomas; both of which affect the complete removal of the gliomas.

Procedures: In this study, the biodistribution of smart matrix metalloproteinase (MMP) targeting near-infrared (NIR) fluorescent probe MMPSense 750 FAST (MMP-750) was examined in both U87MG-GFP-fLuc glioma xenograft and orthotopic mouse models using FMI. Then, CT and FMI images of orthotopic gliomas were acquired for the reconstruction of fluorescence molecular tomography (FMT) using a randomly enhanced adaptive subspace pursuit (REASP) algorithm. Furthermore, the resection of orthotopic glioma was performed using the fluorescence surgical navigation system after the injection of the MMP-750 probe. After surgery, bioluminescence imaging (BLI) and hematoxylin and eosin staining were carried out to confirm the precision resection of the tumor.

Results: FMI results showed that the MMP-750 probe can specifically target U87MG glioma *in vivo*. FMT presented the spatial information of the orthotopic glioma using the REASP reconstruction algorithm. Furthermore, MMP-750 could effectively delineate the tumor margin during glioma surgery leading to a complete resection of the tumors.

Li Li and Yang Du contributed equally to this work.
Electronic supplementary material The online version of this article (https://doi.org/10.1007/s11307-017-1158-7) contains supplementary material, which is available to authorized users.

Correspondence to: Xinjian Chen; *e-mail:* xjchen@suda.edu.cn, Jie Tian; *e-mail:* tian@ieee.org

Published online: 12 April 2018

Conclusions: The smart MMP-750 specifically targets the glioma and FMT of MMP-750 provides 3D information for the spatial localization of the glioma. MMP-750 can work as an ideal fluorescence probe for guiding the intraoperative surgical resection of the glioma, possessing clinical translation.

Key words: Matrix metalloproteinase, Image-guided surgery, Glioma, Fluorescence molecular tomography

Introduction

Malignant glioma, the most common primary brain tumor, accounts for about 2 % of all cancers and represents one of the most life-threatening diseases [1]. Although surgery is usually followed by chemotherapy and radiation therapy, the recurrence rate is extremely high due to residual lesions after the operation, which ultimately leads to the death of patients. Surgeons usually assess tumor boundaries based on their experience during surgery. However, it is difficult to distinguish tumor tissue and normal tissue intraoperatively due to possible micro-invasion of the surrounding tissues, and positive tumor margins can develop in local or locoregional recurrence following surgical therapy. Thus, defining a method to objectively assess tumor margins during surgery is urgently needed for precision medicine [2]. Although anatomical and functional imaging techniques such as positron emission tomography (PET), magnetic resonance imaging (MRI), and computed tomography (CT) have played an important role in accurate preoperative diagnostics, most parts of these techniques cannot be applied intraoperatively [3]. In some cases, intraoperative MRI and CT scanning are used by surgeons, but intraoperative systems are costly and complex for neurosurgery. Ultrasound and X-ray imaging are used during cancer surgery, but these modalities lack the possibility of using targeted contrast agents to specifically visualize certain cell types and expose patients to ionizing radiation [4].

Optical imaging, fluorescence and bioluminescence imaging are emerging imaging modalities that offer high sensitivity, high spatial resolution, low cost, real-time data acquisition and do not use ionization radiation. Optical molecular imaging is a promising technique that provides a high degree of sensitivity and specificity in tumor margin detection, and has received increasing attention in recent years [5]. Fluorescence molecular imaging (FMI), as one of the optical imaging methods, possesses the potential to help distinguish normal and tumor tissues by injecting the fluorescent agent, and is demonstrated as a feasible method for precise intraoperative tumor positioning and guidance of surgery [6–9]. However, the limited penetration depth of FMI prevents its application for deep tumor imaging of gliomas [10]. Fluorescence molecular tomography (FMT) can overcome this problem by taking into account the diffuse nature of photon propagation in tissues, and serves as an ideal technique for detection in deep tissues [11]. FMT can produce accurate tomographic reconstruction and visualization of the deep light source in 3D mode by combining micro-CT and fluorescence images. It is also reported that FMT can resolve protease activity *in vivo*, and FMT has considerable advantages over existing imaging technologies in providing high-throughput functional information in living animals [12].

There is a pressing need to develop new diagnostic imaging agents combined with FMI for the detection of glioma at an early stage and intraoperative detection. Matrix metalloproteinases (MMPs) are expressed in cancers at much higher levels than in normal tissues and the extent of expression has been shown to be correlated with tumor stage, tumor progression [13], invasiveness [14, 15], and metastasis [16]. MMPs degrade collagen IV and further enable the escape of cancer cells to other organs. The fluorescence-labeled MMP probe has been shown to be able to efficiently and abundantly accumulate in tumor areas for targeted tumor imaging [17, 18]. The probe only responds to the tumor microenvironment but not healthy tissues, hence possessing a higher tumor targeting specificity.

In this study, the application of MMP-750 for the targeted fluorescence imaging of orthotopic glioma was initially examined using FMI, and then the FMT of MMP-750 was reconstructed to provide the depth and volumetric information for the glioma *in situ*. Finally, the image-guided intraoperative surgery using MMP-750 agent was performed for the precise resection of the glioma. The tumor residuals after surgery were assessed using GFP and bioluminescence imaging (BLI) and histology. The results of our study suggested that the MMP-750 fluorescent imaging agent facilitates targeted imaging and detection of gliomas and complete removal of gliomas during surgery, realizing precision medicine.

Materials and Methods

Materials and Reagents

A human U87MG glioma cell line was obtained from the American type culture collection (ATCC, USA), and the U87MG cell line was stably transfected with the GFP-luciferase gene (U87-GFP-fLuc). The culture medium and fetal bovine serum (FBS) were purchased from HyClone (Thermo Scientific, USA). D-Luciferin was bought from Biotium (Fremont, CA, USA). MMPSense 750 FAST

(MMP-750) was purchased from PerkinElmer (Waltham, MA, USA).

Cell Culture

Human U87MG-GFP-fLuc glioma cells were cultured in Dulbecco's modified Eagle medium and supplemented with 10 % fetal bovine serum (FBS). The cells were maintained at 37 °C in an incubator with 5 % CO_2.

Experimental Animal Models

All animal experiments were performed in accordance with the guidelines of the Institutional Animal Care and Use Committee (IACUC) at Peking University (Permit No: 2011-0039). The experiments were carried out on 4~5-week-old male BALB/c athymic mice weighing 15–18 g (Vital River Laboratory Animal Technology Corporation, Beijing, China). Purina Chow and water were available *ad libitum*. Ambient temperature was set to 22–23 °C. The subcutaneous tumor model ($n = 20$) was established by injecting 10^7 U87MG cell suspension subcutaneously in the backs of the mice. The orthotopic tumor model ($n = 20$) was established after being anesthetized with sodium pentobarbital, and the mice were attached to the stereotaxic system (David Kopf Instruments, Tujunga, CA). After disinfection and incision of the skin, a midline incision was made through the skin overlying the cranium. A small hole was made in the skull using a bone drill, and then the 10^6 cells were implanted into the brain (2 mm posterior and 2 mm lateral, and 2.5 mm behind the bregma) using a Hamilton syringe (Anting Co. Shanghai, China). The needle was slowly withdrawn after the cell infusion, and the scalp was closed with sutures.

In Vivo Bioluminescent Imaging

The BLI of the glioma was acquired as a reference for the localization of the tumor *in vivo*. Before BLI was acquired, the mice were anesthetized and injected intraperitoneally with D-luciferin (150 mg/kg) for 8 min. The data were then collected with an IVIS Spectrum Imaging System (PerkinElmer, USA).

Biodistribution of the Fluorescent Probe

The MMP-750 probe was reconstituted with 1.2 ml of 1× phosphate-buffered saline (PBS) before intravenous injection of the animals at a dose of 2 nmol (100 μl) per mice. The *in vivo* biodistribution of the MMP750 probe was dynamically monitored using the IVIS Spectrum Imaging System (PerkinElmer, USA) at different time points after intravenous injection.

Micro-CT/FMI System

In order to determine the specific spatial location and brain tumor volume in living mice preoperatively, FMT was implemented using the data obtained from the micro-CT/FMI system. The schematic illustration of the micro-CT/FMI system is shown in Fig. 1a.

The micro-CT/FMI imaging system is located in a dark lead room that can block both external lights and X-rays. The micro-CT system consists of a micro-focus X-ray source (UltraBright, Oxford Instruments, USA). The target voltage of the X-ray tube is 90 kVp. There is a 120 mm × 120 mm photodiode area for the X-ray flat panel detector (C7942CA-02, Hamamatsu, Japan). For the FMI system, it was excited *via* a 749 nm continuous wave laser. The fluorescence image was captured by a near-infrared charged-coupled device camera (VersArray, Princeton Instruments, USA). The reflectance mode was adopted to obtain the fluorescent signal. The excitation angles were set to 0°. It is worth mentioning that they are all mounted on a vertical electric turntable rotating at a uniform speed.

In vivo FMT of the Orthotopic Glioma Model

FMT was implemented on orthotopic glioma mice 24 h after intravenous injection of the MMP-750 probe on the 9th day after the tumor cell implantation. The mice were anesthetized with 2 % isoflurane and placed on a flat plate perpendicular to the turntable. First, the FMI signal was captured by the CCD camera, and then anatomic information was collected using the micro-CT system.

Reconstruction Method

The data processing procedure is shown in Fig. 1b. First, micro-CT and the fluorescence image were preprocessed for the reconstruction of FMT. Four main biological tissues including the brain, lung, heart, and bone were segmented and assembled through CT data. The optical properties of the biological tissues were allocated according to Table 1 [19, 20]. Then, the assembled torso model was meshed using the finite element method, and the image domain was discretized into 3862 nodes and 18,692 tetrahedrons. Third, the measured fluorescent data were mapped onto the mouse surface to complete the energy mapping and registration. Finally, the registration and mesh generation were both performed to realize FMT by the reconstruction algorithm.

From the perspective of compressed sensing, the tumor reconstruction was conducted as sparse signal recovery. Hence, a randomly enhanced adaptive subspace pursuit (REASP) method was utilized for fluorescence tomography reconstruction [21]. REASP adds relative and irrelative atoms with an adaptive technique and a random strategy, respectively. Compared to the general subspace pursuit algorithms, REASP enhances the reconstruction accuracy

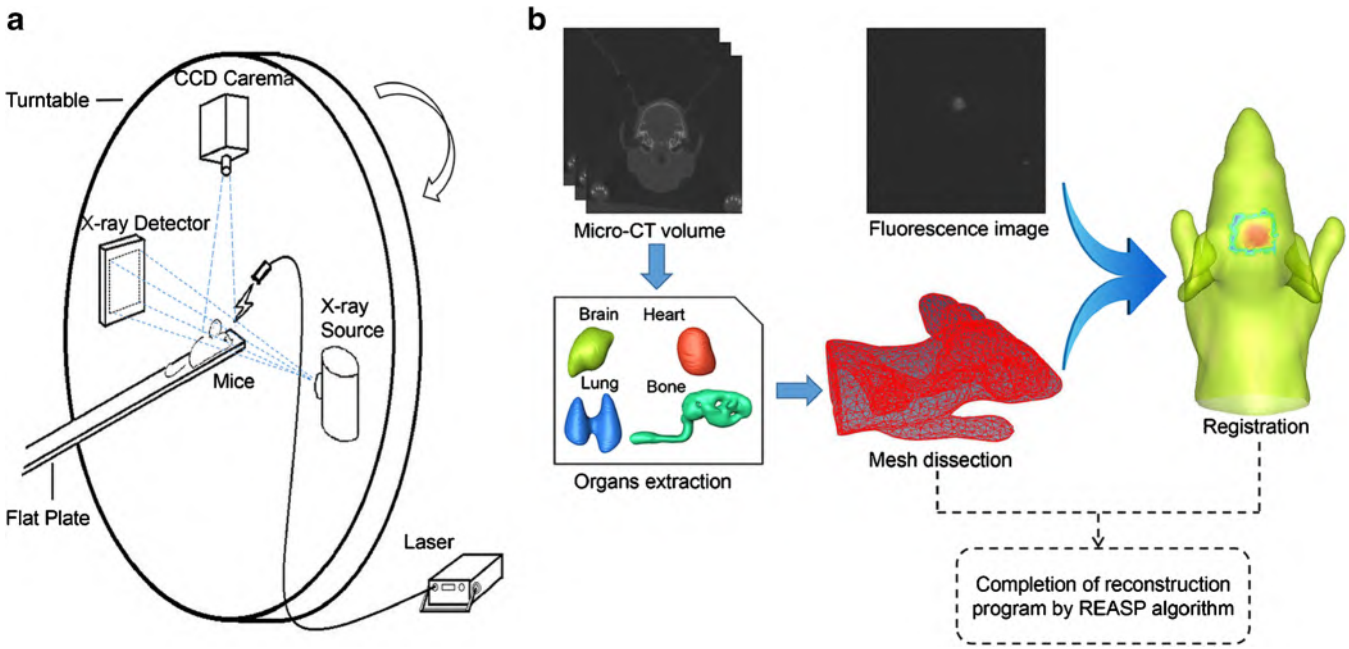

Fig. 1 The main procedures of data acquisition and processing. **a** The scheme of the multimodality imaging system. **b** Data processing for reconstruction of fluorescence molecular tomography.

and robustness. Figure 2 describes the outline of the proposed algorithm.

Where A is a M × N matrix, Φ is a measurement vector, K is a sparsity level, μ is a preset atom-addition parameter threshold, N_{max} is the number of maximum iterations allowed, and q is a preset upper bound of the estimated set's cardinality. Here, μ is set to 0.7, $N_{max} = M$, and $q = 0.8\lceil M \rceil$. $I = \{$indices of K largest absolute value in $A^{\top}\Phi\}$(estimated support set), $x^0 = A_I^{\dagger}\Phi$, $r^0 = \Phi - Ax^0$, $E = \{1,2,\cdots,N\}$ (the whole coordinate set),$S_0 = \phi$, and $D_0 = \phi$.

FMI-Guided Surgery

A total of 20 orthotopic mice were randomly divided into two groups ($n = 10$ per group). For the traditional surgery, surgeons performed surgeries according to their experience and perception without aid of image guidance. For the FMI-guided surgery group, the mice were intravenously injected with the MMP-750 probe, and real-time intraoperative fluorescence image-guided surgery was performed 24 h post-injection under a fluorescence stereomicroscope (Leica, M205 FA, Germany) by surgeons. Mice were imaged by GFP and BLI (PerkinElmer, USA) before and after surgery to detect the tumor residuals.

Table 1. The optical scattering and absorption properties of the mice' tissues at 749 nm (excitation) and 775 nm (emission)

	$\mu_{sx}(m^{-1})$	$\mu_{sm}(m^{-1})$	$\mu_{ax}(m^{-1})$	$\mu_{am}(m^{-1})$
Bone	2118	2015	60.17	52.37
Heart	822	783	59.19	52.26
Lung	2049	2013	190.85	163.88
Muscle	313	285	85.96	74.820
Brain	1262	1195	26.90	26.95

Histological Studies

Mice were euthanized after surgery, and the brain and tumor tissues were excised, fixed, and embedded in paraffin. Continuous sections (4 μm) were obtained and prepared for hematoxylin and eosin (H & E) staining.

Statistical Analysis

The experimental data were analyzed using Prism 5.0 (San Diego, CA, USA). Data were presented as means ± SEM from three independent experiments. One-way analysis of variance (ANOVA) and Tukey's multiple comparison tests or Student's t tests were used to determine significant differences. Differences with P values of less than 0.05 were regarded as statistically significant.

Results

In Vivo MMP-750 Biodistribution

The *in vivo* biodistribution and tumor targeting effect of MMP750 were monitored on glioma xenograft bearing mice with a tumor volume around 100 mm^3 at different time points after the injection of MMP-750. The tumor location is indicated by BLI in Fig. 3a. As shown in Fig. 3b, the fluorescence signal at the tumor site increased gradually

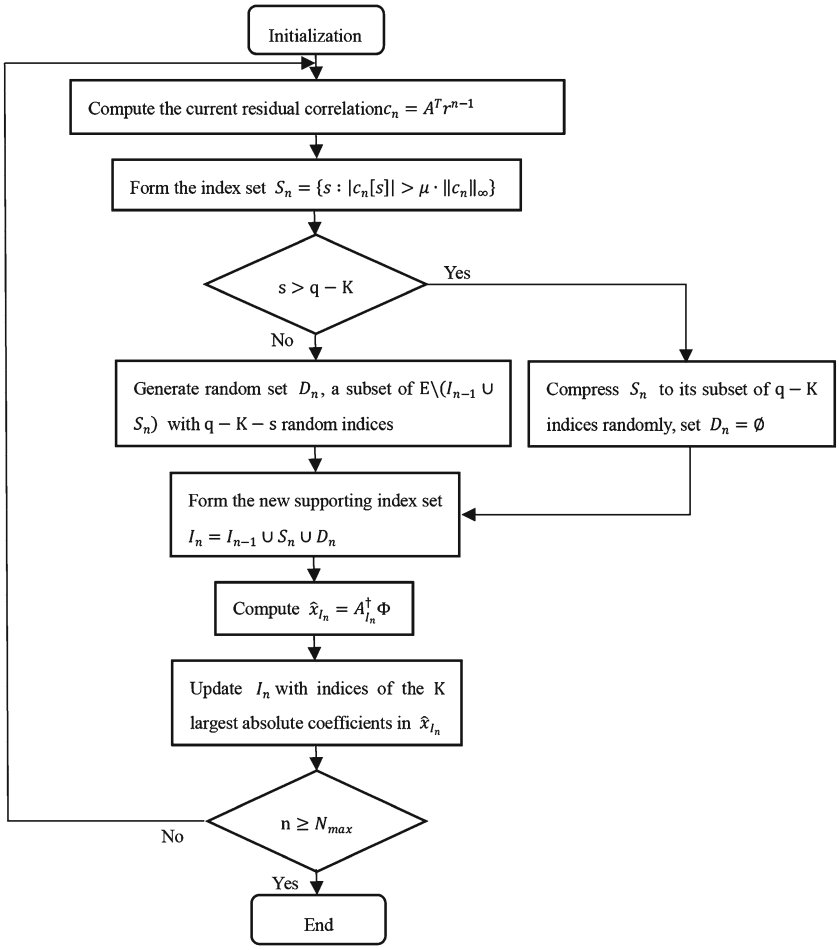

Fig. 2 Diagram for the randomly enhanced adaptive subspace pursuit (REASP) algorithm.

from 1 to 24 h post-injection and FMI revealed good glioma targeting effects. The fluorescence signal was retained for at least 36 h post-injection, and then the intensity decreased thereafter during the observation period. The tumor to background ratio (TBR) of fluorescence imaging was measured and calculated, and the data in Fig. 3c showed the highest ratio was around 24 h post-injection of the MMP-750. Furthermore, 48 h after *in vivo* observation, tumors and major organs of the mice were dissected and processed for the *ex vivo* fluorescence imaging, and the data in Fig. 3d confirmed the specific fluorescence signal in tumors so that no observable fluorescence signal was present in other organs.

The biodistribution of MMP-750 was further examined using FMI on the orthotopic glioma mouse model, which preserves the maximum extent of the cancer's "natural" microenvironment [22, 23]. BLI denotes the glioma location in the brain of tumor-bearing mice (Fig. 3e). As shown in Fig. 3f, the fluorescence signal was observed 1 h post-injection, and gradually increased. The fluorescence signal at the brain tumor area reached a plateau 24 h post-injection and maintained high intensity up to 36 h. The signal then gradually declined thereafter till 48 h. The TBR of FMI was correlated with *in vivo* FMI observation, and the data in Fig. 3g showed the highest TBR around 24–36 h post-injection. The brain and major organs of the mice were dissected 48 h after probe injection, and their fluorescence signals were quantitatively analyzed. As shown in Fig. 3h, the fluorescence signal can be detected in glioma in the brain but not in the other organs. These above results indicated that MMP-750 can realize targeted *in vivo* fluorescence imaging of gliomas.

MMP-750 FMT Reconstruction Results

FMT is a method that three-dimensionally resolves fluorescence biodistribution *in vivo* and serves as an ideal method for deep tissue detection. The FMT reconstruction results of MMP-750 for the orthotopic glioma mouse model were shown in Fig. 4a, b from different views. The images clearly showed that the orthotopic glioma, which was located in the deep part of the brain and also the 3D images of the tumor volume could be clearly visualized as indicted by the arrow. These data can give us comprehensive information for the preoperative evaluation of the glioma compared to FMI.

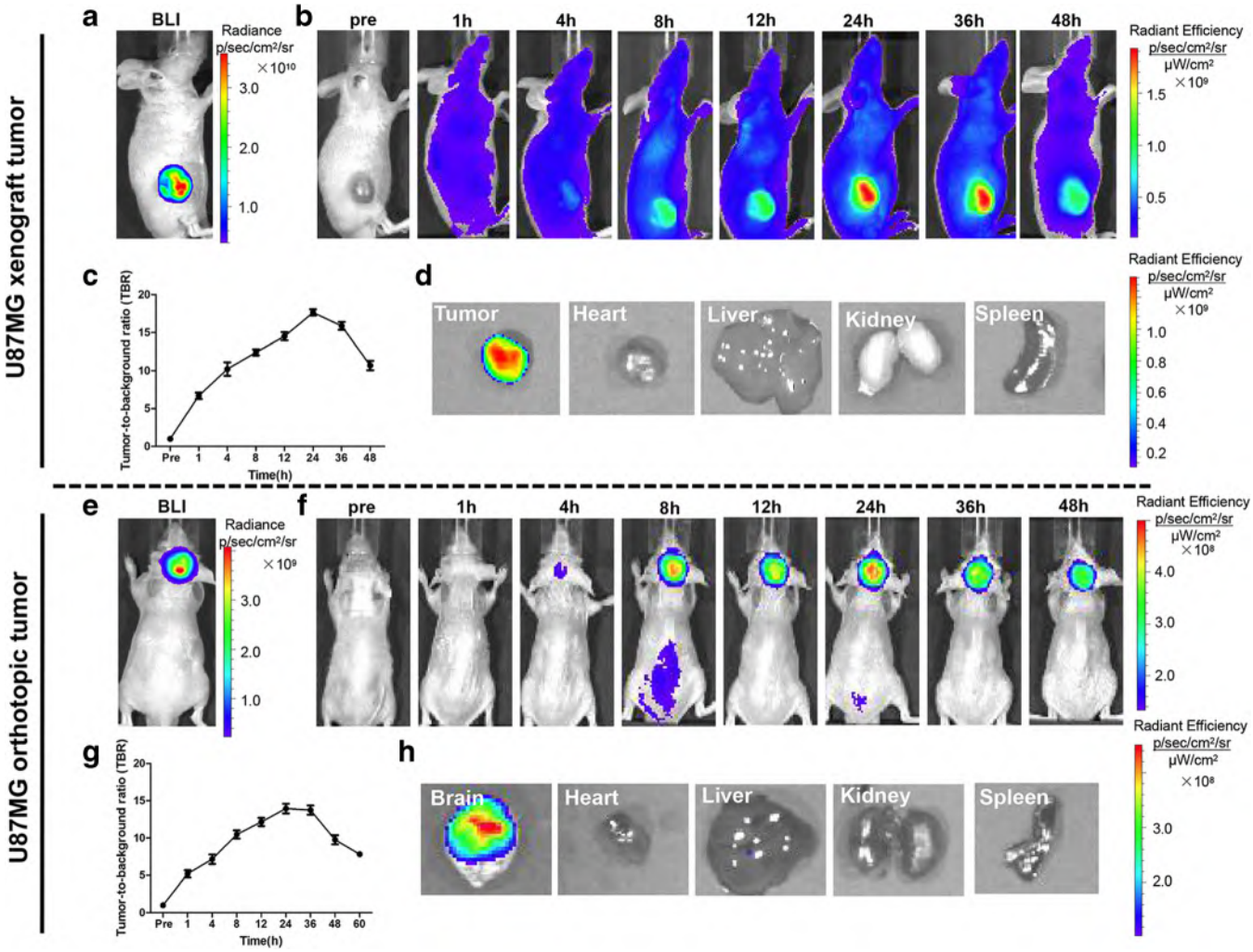

Fig. 3 The biodistribution of MMP-750 in the xenograft and the orthotopic glioma mouse model. **a** BLI of the glioma xenograft. **b** Continuous FMI observation of the glioma xenograft model. **c** The tumor-to-background ratio (TBR) of FMI for the glioma xenograft-bearing mouse. **d***Ex vivo* fluorescence images of the dissected tumor and major organs at 48 h after the probe injection. **e** BLI of the orthotopic glioma mouse model. **f** The dynamic fluorescence signal distribution of the orthotopic glioma mouse model at different time points. **g** The tumor-to-background ratio (TBR) of FMI for orthotopic glioma mice. **h***Ex vivo* fluorescence images of the dissected brain and major organs 48 h after the probe injection.

Intraoperative Detection and Resection of Glioma by the Surgical Navigation System

FMI-guided intraoperative detection and resection of the glioma 24 h after intravenous injection of MMP-750 is shown in Fig. 5. Figure 5a–c depicts the fluorescence imaging of tumors in the preoperative condition, and the tumor can be clearly visualized *in situ* through NIRF imaging. Figure 5d–f shows the image-guided resection of the tumors, and even the small tumor residual can be detected intraoperatively. Figure 5g–i shows the postoperative condition, where the tumor was completely removed. The resected tumor is shown in Fig. 5j–l. Figure 5a–j are color images. Figure 5b–k are fluorescent images. Figure 5c–l are the overlayed images of fluorescence and color images. The data suggested that FMI-guided surgery by MMP-750 was feasible for the complete resection of the glioma.

Comparison Between FMI-Guided Surgery and Traditional Surgery

Furthermore, FMI-guided surgery and traditional surgery of gliomas for precision resection was further compared in Fig. 6. First, GFP imaging of the U87MG-GFP-fLuc glioma was performed to examine the tumor residuals. Figure 6a–f shows the color and GFP images of gliomas performed by image-guided surgery. Figure 6a–c shows the preoperative

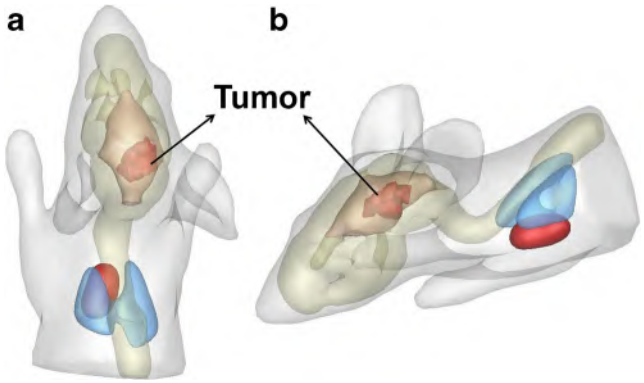

Fig. 4 FMT reconstruction results of orthotopic glioma-bearing mice from the frontal (**a**) and side views (**b**).

condition and GFP image depicting the tumor location in the brain. Figure 6d–f shows the postoperative situation, where there was no GFP signal left after FMI-guided surgery. Figure 6g–l shows the color and GFP images of gliomas *via* traditional surgery. igure 6g–i exhibits the preoperative condition and Fig. 6j–l shows the postoperative situation. GFP positive glioma cells can be found after the traditional surgery, suggesting there were tumor cell residuals after surgery. Second, the BLI of U87MG-GFP-fLuc glioma was performed to examine the tumor residuals. FFigure 6m, o shows the location of the orthotopic gliomas for both FMI-guided surgery and traditional surgery groups. Similar to the GFP image results, there was no BLI signal after FMI-guided surgery in Fig. 6n, but some BLI can be found after the traditional surgery as shown in Fig. 6p. Third, the histological analyses were further performed to confirm the tumor residuals after the surgery as shown in Fig. 6q–s. As shown in Fig. 6r, the positive tumor margin can be identified adjacent to the normal brain tissue in the traditional surgery group, but not in the FMI-guided surgery group. The data in general indicated that the MMP-750 probe in combination with FMI-guided surgery can improve the precision resection of glioma *in situ*.

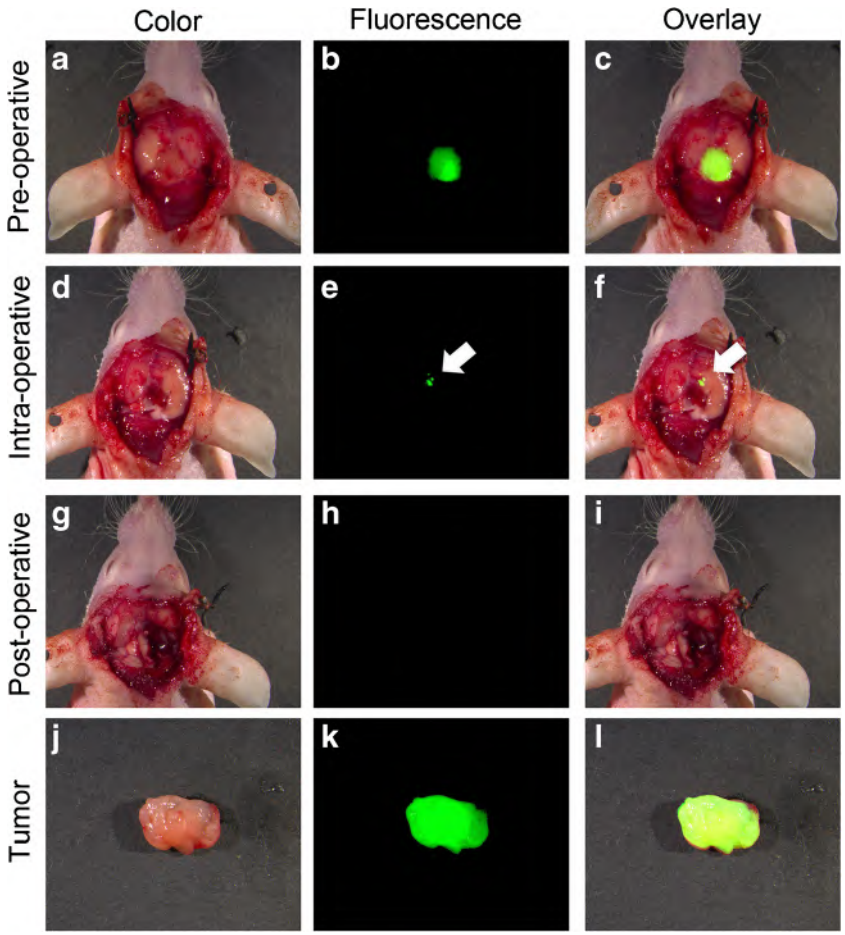

Fig. 5 FMI-guided intraoperative detection and resection of a glioma. The first row is the preoperative condition. The second row represents the intraoperative situation, and the third row is the postoperative condition. The last row shows the dissected tumors. **a**, **d**, **g**, and **j** are color images. **b**, **e**, **h**, and **k** are fluorescence images. **c**, **f**, **i**, and **l** are the overlayed images generated by merging the fluorescence image and the color image.

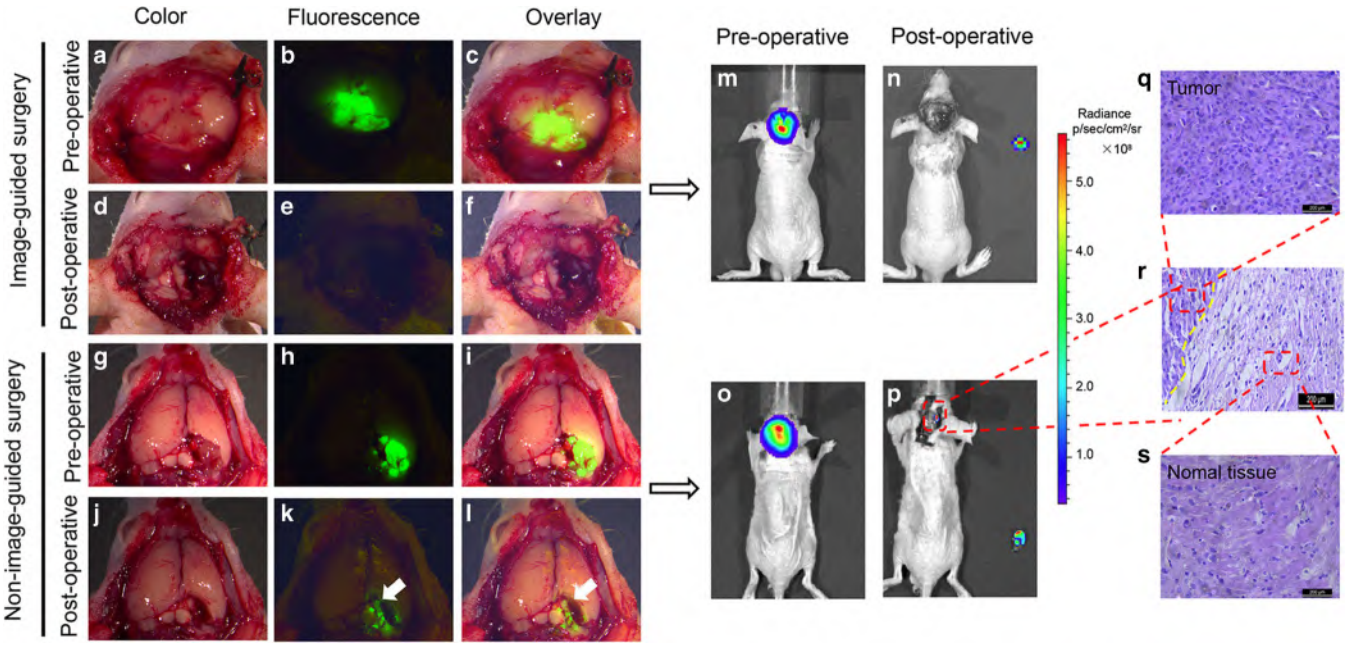

Fig. 6 **a**–**l** Evaluation of the tumor residuals after surgery. **a**–**l** represent GFP imaging for the evaluation of tumor residuals. The first two rows show the FMI-guided surgery. **a**–**c** include the preoperative condition, **d**–**f** are the postoperative situation, and the last two rows are non-image-guided surgery. **g**–**i** are the preoperative condition and **j**–**l** are the postoperative situation. **a**, **d**, **g**, and **j** are color images. **b**, **e**, **h**, and **k** are fluorescence images. **c**, **f**, **i**, and **l** are the overlayed images generated by merging of a fluorescence image and a color image. **m**–**p** are the bioluminescence images (BLI) of orthotopic glioma for the evaluation of the tumor residuals. **m**, **o** are the preoperative BLI images and **n**, **p** are the postoperative BLI images. **q**–**s** include the hematoxylin and eosin (H & E) evaluation of the tumor residuals. **q** shows the tumor section. **r** shows the tumor margin. **s** shows the normal surrounding tissues.

Discussion

Glioma is the most malignant primary brain tumor with a rapid tumor progression. Glioma is characterized by extensive invasion into the surrounding normal brain tissues, which results in recurrence near the resection margins [24, 25]. Early diagnosis and treatment often extend the quality and survival for individuals suffering with glioma. Optical molecular imaging has become an increasingly important aspect of medical imaging due to its high degree of sensitivity and specificity in tumor imaging [26]. Fluorescence molecular imaging (FMI) can enhance visualization, characterization, and quantification of biological processes *in vivo* [27]. Lately, FMI has been demonstrated experimentally, a crucial step towards its application in intraoperative image-guided tumor surgery by combining it with a tumor-targeted imaging agent [28]. However, FMI imaging modality shows limited penetration depth of the tumor [10]. FMT can provide the depth and three-dimensional information for deep tumors inside of the body and can facilitate comprehensive preoperative assessment of gliomas. An important advantage to potential clinical tomographic imaging is the fact that FMT is inherently quantitative. Other advantages include no ionizing radiation, no decay of the beacons and fluorochromes, and it is relatively inexpensive compared with other tomographic imaging systems [12]. The human brain is a delicate organ, and it may cause loss of brain function, such as dementia and paralysis, if removed arbitrarily during surgery [29]. Since FMT can provide the accurate location and volumetric information for deep tumors inside of the brain, it can help surgeons to determine whether the tumor area is the functional area in the brain and assess whether surgery will affect the patient's prognosis. Although MRI is commonly used preoperatively in clinics, FMT is more sensitive compared to MRI for early detection of carcinogenesis [30, 31]. The idea of using FMT imaging preoperatively can provide a reference for clinical practice in the future.

As an essential component of FMI, molecular-specific contrast agents are required for the imaging of molecular features of glioma *in vivo*. MMPs are known to be expressed in the tumor microenvironment and play an important role in regulating glioma progression [32]. Additionally, it is feasible to image MMP enzyme activity *in vivo* by using near-infrared fluorescence imaging technology and "smart" matrix metalloproteinase-sensitive probes [17, 18]. Hence, the near-infrared dye-labeled MMP-750 was utilized in this study as a tumor-targeted fluorescent probe and we explored its application for intraoperative FMI-guided glioma resection.

In the current study, *in vivo* FMI of MMP-750 for targeted imaging of a glioma was performed. FMT was further performed preoperatively to get the penetration depth and 3D tumor volume information. To fulfill these aims,

subcutaneous and orthotopic glioma models were established using a human U87MG-GFP-fLuc glioma cell line. Tumor-bearing mice were administered the MMP-750 probe to examine its potential for targeted glioma imaging. FMT was reconstructed by the micro-CT/FMI system to exhibit the 3D image and the spatial location of the tumor in the brain before surgery. FMI-guided surgery in combination with the MMP-750 imaging agent was then carried out on an orthotopic glioma. After surgery, three approaches were performed to examine the tumor residuals. First, GFP imaging of the U87MG-GFP-fLuc glioma was performed to examine the tumor residuals. Second, BLI of the U87MG-GFP-fLuc glioma was performed to examine the tumor residuals. The GFP and BLI imaging results showed that the GFP and BLI signals cannot be detected after FMI-guided surgery, while the GFP and BLI positive glioma cells can be found after traditional surgery suggesting that FMI-guided surgery is better than traditional surgery. Third, the histological analyses were further performed to confirm the tumor residuals after surgery. These confirmatory experiments demonstrated that MMP-750 probes in combination with FMI-guided surgery can improve the precision resection of gliomas.

Conclusion

In conclusion, the FMI findings suggested that MMP-750 is able to specifically target gliomas *in vivo*. FMT reconstruction can provide 3D quantitative imaging of the fluorescent source distribution inside the glioma, which can provide surgeons with preoperative information of the tumor volume and location inside of the brain. Compared to the traditional surgery, MMP-750 image-guidance helps surgeons distinguish normal and malignant glioma tissues, thereby increasing the precision resection of surgery and potentially decreasing tumor recurrence. Our future direction will focus on how to display FMT in real time intraoperatively, and combine magnetic resonance imaging (MRI) and FMT to get more accurate spatial information of tumors *in vivo*. As a result, tumor fluorescence derived from MMP-750 can be used for the guidance of glioma resection by surgeons in real time. MMP-750 is currently used for research only and is not allowed for clinical purposes. More efforts will be made to develop similar MMP-targeted fluorescence probes to pass FDA requirements for future clinical application.

Acknowledgements. The authors thank Adjunct Assistant Professor Dr. Karen M. von Deneen from the University of Florida for her English editing of this paper.

Funding Information. This work was supported by the National Natural Science Foundation of China (81227901, 81470083, 81527805, and 61231004), the Research and Development Program of China (973) under Grant (2014CB748600, 2015CB755500), the Strategic Priority Research Program from the Chinese Academy of Sciences under Grant No. XDB02060010, the International Innovation Team of CAS under Grant No. 20140491524, Beijing Municipal Science & Technology Commission No. Z161100002616022, and Beijing Natural Science Foundation (Z16110200010000).

Compliance with Ethical Standards.

All animal experiments were performed in accordance with the guidelines of the Institutional Animal Care and Use Committee (IACUC) at Peking University (Permit No.: 2011-0039).

Conflict of Interests

The authors declare that they have no conflict of interest.

References

1. Avgeropoulos NG, Batchelor TT (1999) New treatment strategies for malignant gliomas. Oncologist 4(3):209–224
2. Nguyen QT, Olson ES, Aguilera TA, Jiang T, Scadeng M, Ellies LG, Tsien RY (2010) Surgery with molecular fluorescence imaging using activatable cell-penetrating peptides decreases residual cancer and improves survival. PNAS 107(9):4317–4322. https://doi.org/10.1073/pnas.0910261107
3. Chi C, Du Y, Ye J, Kou D, Qiu J, Wang J, Tian J, Chen X (2014) Intraoperative imaging-guided cancer surgery: from current fluorescence molecular imaging methods to future multi-modality imaging technology. Theranostics 4(11):1072–1084. https://doi.org/10.7150/thno.9899
4. Vahrmeijer AL, Hutteman M, Vorst JRVD et al (2013) Image-guided cancer surgery using near-infrared fluorescence. Nat Rev Clin Oncol 10(9):507–518. https://doi.org/10.1038/nrclinonc.2013.123
5. Ntziachristos V, Ripoll J, Wang LV, Weissleder R (2005) Looking and listening to light: the evolution of whole-body photonic imaging. Nat Biotechnol 23(3):313–320. https://doi.org/10.1038/nbt1074
6. Nguyen QT, Tsien RY (2013) Fluorescence-guided surgery with live molecular navigation—a new cutting edge. Nat Rev Cancer 13(9):653–662. https://doi.org/10.1038/nrc3566
7. van Dam GM, Themelis G, Crane LM, Harlaar NJ, Pleijhuis RG, Kelder W, Sarantopoulos A, de Jong JS, Arts HJ, van der Zee AG, Bart J, Low PS, Ntziachristos V (2011) Intraoperative tumor-specific fluorescence imaging in ovarian cancer by folate receptor-α targeting: first in-human results. Nat Med 17(10):1315–1319. https://doi.org/10.1038/nm.2472
8. Vorst JRVD, Schaafsma BE, PhD MHM et al (2013) Near-infrared fluorescence-guided resection of colorectal liver metastases. Cancer 119(18):3411–3418. https://doi.org/10.1002/cncr.28203
9. Sugie T, Sawada T, Tagaya N, Kinoshita T, Yamagami K, Suwa H, Ikeda T, Yoshimura K, Niimi M, Shimizu A, Toi M (2013) Comparison of the indocyanine green fluorescence and blue dye methods in detection of sentinel lymph nodes in early-stage breast cancer. Ann Surg Oncol 20(7):2213–2218. https://doi.org/10.1245/s10434-013-2890-0
10. Virostko J, Powers AC, Jansen ED (2007) Validation of luminescent source reconstruction using single-view spectrally resolved bioluminescence images. Appl Opt 46(13):2540–2547. https://doi.org/10.1364/AO.46.002540
11. Deliolanis NC, Ntziachristos V (2013) Fluorescence molecular tomography of brain tumors in mice. Cold Spring Harb Protoc 2013:438
12. Ntziachristos V, Tung CH, Bremer C, Weissleder R (2002) Fluorescence molecular tomography resolves protease activity in vivo. Nat Med 8(7):757–761. https://doi.org/10.1038/nm729
13. Stearns ME, Wang M (1993) Type IV collagenase (M(r) 72,000) expression in human prostate: benign and malignant tissue. Cancer Res 53(4):878–883
14. Davies B, Waxman J, Wasan H et al (1993) Levels of matrix metalloproteases in bladder cancer correlate with tumor grade and invasion. Cancer Res 53:5365
15. Zucker S, Hymowitz M, Conner C et al (1999) Measurement of matrix metalloproteinases and tissue inhibitors of metalloproteinases in blood and tissues: clinical and experimental applications. Ann N Y Acad Sci 878(1 INHIBITION OF):212–227. https://doi.org/10.1111/j.1749-6632.1999.tb07687.x
16. Moses MA, Wiederschain D, Loughlin KR, Zurakowski D, Lamb CC, Freeman MR (1998) Increased incidence of matrix metalloproteinases in urine of cancer patients. Cancer Res 58(7):1395–1399

17. Bremer C, Bredow S, Mahmood U, Weissleder R, Tung CH (2001) Optical imaging of matrix metalloproteinase-2 activity in tumors: feasibility study in a mouse model. Radiology 221(2):523–529. https://doi.org/10.1148/radiol.2212010368
18. Chi C, Zhang Q, Mao Y, Kou D, Qiu J, Ye J, Wang J, Wang Z, du Y, Tian J (2015) Increased precision of orthotopic and metastatic breast cancer surgery guided by matrix metalloproteinase-activatable near-infrared fluorescence probes. Sci Rep 5(1):14197. https://doi.org/10.1038/srep14197
19. Jacques SL (2013) Optical properties of biological tissues: a review. Phys Med Biol 58(11):R37–R61. https://doi.org/10.1088/0031-9155/58/11/R37
20. Alexandrakis G, Rannou FR, Chatziioannou AF (2005) Tomographic bioluminescence imaging by use of a combined optical-PET (OPET) system: a computer simulation feasibility study. Phys Med Biol 50(17):4225–4241. https://doi.org/10.1088/0031-9155/50/17/021
21. Liu L, Du X, Cheng L (2013) Stable signal recovery via randomly enhanced adaptive subspace pursuit method. IEEE Signal Processing Letters 20:823–826
22. Killion JJ, Radinsky R, Fidler IJ (1998) Orthotopic models are necessary to predict therapy of transplantable tumors in mice. Cancer Metastasis Rev 17(3):279–284. https://doi.org/10.1023/A:1006140513233
23. Hu H, Liu J, Yao L et al (2012) Real-time bioluminescence and tomographic imaging of gastric cancer in a novel orthotopic mouse model. Oncol Rep 27:1937
24. Furnari FB, Fenton T, Bachoo RM, Mukasa A, Stommel JM, Stegh A, Hahn WC, Ligon KL, Louis DN, Brennan C, Chin L, DePinho RA, Cavenee WK (2007) Malignant astrocytic glioma: genetics, biology, and paths to treatment. Genes Dev 21(21):2683–2710. https://doi.org/10.1101/gad.1596707
25. Wen PY, Kesari S (2008) Malignant gliomas in adults. NEJM 359(5):492–507. https://doi.org/10.1056/NEJMra0708126
26. Sokolov K, Aaron J, Hsu B, Nida D, Gillenwater A, Follen M, MacAulay C, Adler-Storthz K, Korgel B, Descour M, Pasqualini R, Arap W, Lam W, Richards-Kortum R (2003) Optical systems for in vivo molecular imaging of cancer. Technol Cancer Res Treat 2(6):491–504. https://doi.org/10.1177/153303460300200602
27. Cheong SJ, Lee CM, Kim EM, Uhm TB, Jeong HJ, Kim DW, Lim ST, Sohn MH (2011) Evaluation of the therapeutic efficacy of a VEGFR2-blocking antibody using sodium-iodide symporter molecular imaging in a tumor xenograft model. Nucl Med Biol 38(1):93–101. https://doi.org/10.1016/j.nucmedbio.2010.05.009
28. Ntziachristos V (2006) Fluorescence molecular imaging. Annu Rev Biomed Eng 8(1):1–33. https://doi.org/10.1146/annurev.bioeng.8.061505.095831
29. Alimohamadi M, Shirani M, Shariat-Moharreri R et al (2016) Application of awake craniotomy and intraoperative brain mapping for surgical resection of insular gliomas of the dominant hemisphere. World Neurosurg 92:151–158. https://doi.org/10.1016/j.wneu.2016.04.079
30. Weissleder R (1999) Molecular imaging: exploring the next frontier. Radiology 212(3):609–614. https://doi.org/10.1148/radiology.212.3.r99se18609
31. Ale A, Ermolayev V, Deliolanis NC, Ntziachristos V (2013) Fluorescence background subtraction technique for hybrid fluorescence molecular tomography/x-ray computed tomography imaging of a mouse model of early stage lung cancer. J Biomed Opt 18(5):56006. https://doi.org/10.1117/1.JBO.18.5.056006
32. Kessenbrock K, Plaks V, Werb Z (2010) Matrix metalloproteinases: regulators of the tumor microenvironment. Cell 141(1):52–67. https://doi.org/10.1016/j.cell.2010.03.015